Self-sputtering far above the runaway threshold: an extraordinary metal ion generator

Joakim Andersson and André Anders

Lawrence Berkeley National Laboratory, 1 Cyclotron Road, Berkeley, California 94720

Abstract

When self-sputtering is driven far above the runaway threshold voltage, energetic electrons are made available to produce "excess plasma" far from the magnetron target. Ionization balance considerations show that the secondary electrons deliver the necessary energy to the "remote" zone. Thereby, such a system can be an extraordinarily prolific generator of useable metal ions. Contrary to other known sources, the ion current to a substrate can exceed the discharge current. For gasless self-sputtering of copper, the useable ion current scales exponentially with the discharge voltage.

PACS: 52.25.Jm, 52.40.Hf, 52.80.Vp, 81.15.Cd, 81.15.Ef, 81.15.Jj

Large fluxes of ions are of interest to a number of plasma-based technologies such as self-ion assisted deposition of films and high-current and large-area ion sources. The generation of large ion fluxes is a challenging task because plasma systems tend to produce just as many ions as necessary to maintain the discharge. Hence, only a small fraction of the generated ions can be utilized for processing. Among the most prolific generators of ions are cathodic arc discharges, where the available ion current is generally quantified by normalizing it to the discharge current; the ratio is typically about 0.1 [1]. In this contribution we will demonstrate that high power impulse magnetron sputtering (HIPIMS) can be an extremely prolific generator of metal ions that, under certain conditions, can deliver ion currents that even exceed the discharge current. We will show that this very high level is consistent with common particle and energy balance considerations.

HIPIMS was developed with the goal to at least partially ionize the sputtered atoms and thereby to provide a means for self-ion assisted deposition of thin films [2-5]. In HIPIMS, and depending on several parameters such as power density, target material and gas pressure, the magnetron discharge plasma contains a large fraction of ionized sputtered material, and therefore HIPIMS processes are closely related to self-sputtering. Self-sputtering is an intriguing subject of research since the early reports by Hoskoawa and coworkers [6, 7] because, after initiating the magnetron in a gas atmosphere at high power density, self-sputtering can sustain itself for a few target materials under certain conditions [8, 9].

The *current-voltage-time* characteristics of HIPIMS discharges in background gas [10, 11] show that for sufficiently long pulses (typically > 100 μs) at constant voltage, the current may go through a maximum and then settle at an equilibrium value. The current reduction after the initial peak is due to gas rarefaction. However, if the power density is high, the current evolution may look completely different in that, at a well-defined voltage threshold, the current does not reduce but jumps to a new, much higher value. This is the threshold of sustained self-sputtering [7]. At the threshold, self-sputtering amplifies itself and the self-sputtering parameter exceeds unity, $\Pi \equiv \alpha\beta\gamma_{SS} > 1$, where α is the probability that a sputtered atoms is ionized, β is the probability that the newly formed ion returns to the target, and γ_{SS} is the self-sputtering yield. All three quantities are time dependent but the system evolves towards a new steady state, with $\Pi = 1$, provided the power supply can supply the necessary current at constant voltage.

Copper is a preferred material for studying sustained self-sputtering because the sustained situation, $\Pi = 1$, can be obtained at manageable, relative low power densities (e.g., ~ 1 kW/cm^2 averaged over the target area). Recently, it was shown that copper allows gasless (high vacuum) self-sputtering to occur in a sustained manner when the magnetron discharge pulses are "kickstarted" via short vacuum arc plasma pulses [12]. We will focus here on "gasless" sputtering because it avoids the modeling complications associated with plasmas containing both gas and metal species.

The current to a negatively biased ion collector, i.e. large probe operating in the ion saturation current, is given by the area integral over the current density $I_i = \int j_i dA$, with the Bohm current [13]

$$j_i = 0.61 n_{i0} \overline{Q} e \left(\frac{kT_{e0}}{m_i} \right)^{1/2}, \tag{1}$$

where n_{i0} is the ion density at the edge of the sheath (index "0") of the collector, $\overline{Q}$ is the mean ion charge state number, e is the elementary charge, $\left(kT_{e0}/m_i\right)^{1/2}$ is the local ion sound velocity which depends on the electron temperature, T_{e0}, and the ion mass; k is the Boltzmann constant. In the derivation of (1), the magnetic field was neglected, and it is assumed that the collector is flat, i.e., that the sheath is much thinner than the collectors curvature. There are ample descriptions of refinement in the literature [14, 15] but this approximation will suffice to discuss the physics.

To determine the ion density in (1), we should consider the ion balance equation at the collector's sheath edge (omitting the index 0 for simplicity)

$$\frac{\partial n_i}{\partial t} = K_\alpha n_a n_e - K_\beta n_e^2 n_i - \nabla \left(n_i \mathbf{v}_i \right) \tag{2}$$

where K_α and K_β are the ionization and recombination coefficients, and the last term describes the plasma flow due to diffusion and drift. The coefficients are [16, 17]

$$K_\alpha = \int f_e(E)\, E^{1/2}\, \sigma_{ea}(E)\, dE \tag{3}$$

$$K_\beta \approx \frac{4}{9}\left(\frac{2\pi}{m_e}\right)^{1/2}\left(\frac{e^2}{4\pi\varepsilon_0}\right)^5 (kT_e)^{-9/2}. \tag{4}$$

where E is the electron energy, $f_e(E)$ is the electron energy distribution function, and σ_{ea} is the ionization cross section. The atomic structure appears in the ionization formula (via σ_{ea}) but the recombination coefficient is only dependent on the temperature because recombination occurs into the upper bound levels which are always hydrogen-like; for this estimate one can use $K_\beta \approx 3\times10^{-39}T_e^{-9/2}$ with K_β in m^6/s and T_e in eV. If we now look at the ionization caused by the energetic tail of Maxwellized (plasma bulk) electrons, i.e. electrons with energies just exceeding the first ionization energy of the atom, E_{01}, we can use the Maxwell distribution in (3) and approximate the cross section by the linear function $\sigma_{ea}(E) \approx C_{ea}(E - E_{01})$, resulting in [17]

$$K_\alpha \approx \left(\frac{8kT_e}{\pi m_e}\right)^{1/2} C_{ea}(E_{01} + 2kT_e)\exp\left(-\frac{E_{01}}{kT_e}\right) \tag{5}$$

where $C_{ea} \approx 5\times10^{-21}$ m^2/eV and $E_i(Cu) = 7.73$ eV. A comparison of ionization and recombination rates shows that ionization is prevalent unless the electron temperature is less than 1 eV (Fig. 1). If we consider that $f_e(E)$ contains a non-Maxwellian component at high energy caused by the secondary electrons accelerated in the sheath of the cathode, one can state that the dominance of ionization is even stronger than Fig. 1 indicates. For steady state, when $\partial n_i/\partial t = 0$, the flux of ions therefore needs to match the "excess" production of ions, leading to

$$K_\alpha n_a n_e - \nabla(n_i \mathbf{v}_i) = 0. \tag{6}$$

Using Gauss' theorem $\oiint \mathbf{D}\, dA = \int_V \nabla\mathbf{D}\, dV$, where $\mathbf{D}$ is any vector field, we can integrate (6) over a volume V of interest (with surface area A):

$$\int_V K_\alpha n_a n_e dV = \oiint n_i \mathbf{v}_i\, dA. \tag{7}$$

The left hand side is the production of ions in the volume V and the right hand side is the flux of ions through the surface A of the volume under consideration.

Following similar lines of thought by others [7, 18, 19], a fraction of the metal ions, β, will return to the target ($0 \le \beta \le 1$). This fraction will mainly depend on the slowing of the fast sputtered atoms by other particles [20], which are mainly neutrals, and thus $\beta(n_a)$. In the case of self-sputtering-dominated steady state, the neutrals are created by self-sputtering, the yield of which depends strongly on the voltage, U, and hence we have $\beta\left(n_a\left(\gamma_{SS}(U)\right)\right)$.

Of the remaining fraction, $(1-\beta)$, a portion δ can be associated with the available ion current at a substrate or collector. The flux fraction $(1-\beta)(1-\delta)$ is "lost" by condensing on the anode or not captured by the ion collector. Using the relation between ion flux and current density,

$$\mathbf{j}_i = eQn_i\mathbf{v}_i \ , \tag{8}$$

we can write for the current at the ion collector

$$I_{i,collect} = (1-\beta)\delta e\overline{Q}\int_V K_\alpha n_e n_a dV \ . \tag{9}$$

For an estimate, we can consider a volume V_0 where the plasma is produced, and, neglecting any non-uniformity within V_0 and taking (5) into account,

$$I_{i,collect} = (1-\beta)\delta e\overline{Q}V_0\left(\frac{8kT_e}{\pi m_e}\right)^{1/2} C_{ea}\left(E_{01}+2kT_e\right)\exp\left(-\frac{E_{01}}{kT_e}\right)n_e n_a \ . \tag{10}$$

The most sensitive dependence is the exponential term in T_e^{-1}, which depends on both the voltage (electron heating) and the density of neutrals (electron cooling). Therefore, as the voltage is increased and more power is dissipated, the electron temperature is likely to increase and the useable ion current increases, too, with an approximate exponential dependence: $I_{i,collect} \sim \exp\left(kT_e(U)/E_{01}\right)$.

To test this hypothesis, a HIPIMS system was used as previously described for operation in gas [10] and in the "gasless" mode [12]. The HIPIMS discharge was fed by an upgraded SPIK2000A pulse power supply (Melec) charged via a Pinnacle DC-supply by Advanced Energy. We focus on the case of "gasless" sputtering at the base

pressure of 10^{-4} Pa with the magnetron pulses of typically 400 μs initiated by short (~20 μs), ~200 A, vacuum-arc discharges [12]. The magnetic induction component parallel to the surface on the surface over the "racetrack" was $B_{\|} = 65$ mT .

The large-area ion collector in the present experiment was a metal cylinder of 15 cm diameter and 16 cm length; it was closed at one side. The magnetron was placed at the "entrance" end of the collector such that practically all ions leaving the magnetron area can be collected ($\delta \approx 1$). The collector was biased negatively with respect to the grounded anode. A stable bias voltage during the HIPIMS pulse was ensured by using a large (5 mF) capacitor. The bias voltage was varied in the range 0-100 V to determine saturation and to study the influence of the bias, if any, on the HIPIMS discharge. The discharge and ion collector currents were measured with suitable broad band current transformers (Pearson). The potentials of the target and the ion collector were monitored by fast voltage dividers (Tektronix). All data were recorded on a digital oscilloscope (Tektronix TDS5104B).

Considering a copper magnetron discharge in vacuum, a minimum voltage of about 600 V was required to obtain a stable discharge (magnetrons with stronger magnetic fields may operate at lower voltages). Fig. 2 shows the current to the ion collector as a function of time for different collector bias voltages. For a bias of just a few volts, electrons can reach the collector, especially in the early, pre-steady-state phase of the discharge. For negative voltages as low as 10 V, most electrons are prevented from reaching the collector; the strongest slope of change, $dI_{i,collect}/dU_{bias}$, is directly indicative for the electron temperature (~ 3 eV). A more precise evaluation of the electron temperature requires the knowledge of the difference of the plasma potential relative to ground, our reference potential. The plasma potential is sensitively affected by the local charge balance, and this explains the time dependence of the collector current at the beginning and end of the pulse. We are interested in ion saturation, which is ensured at all times when the bias is set to about -20 V or greater. One should note that the ion saturation current exceeds the discharge current, which will be discussed below.

We noted that even with -100 V bias at the collector, the magnetron discharge was unchanged within about 5%. This is reasonable given that the power dissipation of the collector circuit is less than 5% of the magnetron power when the bias is set to -30 V, the standard used in our experiments. Furthermore, results were cross-checked with a large *planar* detector.

The discharge and ion collector currents have very similar shapes and so here we display the ion collector current only (Fig. 3). The discharge voltage was increased in steps of 40 V, and one can clearly see that the increase in ion current is greater than proportional. The increase in both discharge current and collector current is exponential if plotted against the discharge voltage (Fig. 4). The threshold of sustained self-sputtering is at the left end of the curves; we see that the available ion current can greatly exceed the discharge current as the discharge is driven far beyond the threshold. The upper (right) end of the curves is limited by frequent arcing events: arcing represents the practical limit of how far the system can be pushed from the threshold of self-sputtering.

As mentioned before, the ions produced in the volume V_0 in front of the target give rise to three fluxes: the ion current going to the target, the ion current going to the collector, and the remaining current going elsewhere. The measured discharge and collector currents are dominated by the arriving ions but we also need to consider the secondary electrons emitted by primary ion impact, leading to $I_i = I_{disch}/(1+\gamma_{SE})$ and $I_{i,collect} = I_{collect}/(1+\gamma_{SE})$. The yield of secondary electrons, γ_{SE}, is dominated by potential emission at the relatively low kinetic energies relevant to magnetron sputtering [21]; singly charged metal ions have a very small yield, and therefore the fraction of multiply charged ions is mainly responsible for the secondary emission [22]. For estimates, we preliminary could use an effective yield of $\gamma_{SE} \approx 0.05$, a reasonable value, as will be shown below. Then we can utilize the measurements of discharge current and collector current to approximately determine the return probability β:

$$\beta = \frac{I_{disch}/(1+\gamma_{SE})}{I_{disch}/(1+\gamma_{SE}) + I_{collect}/(1+\gamma_{SE}) + I_{lost}} \approx 0.95\frac{I_{disch}}{I_{disch}+I_{collect}}. \quad (11)$$

Fig. 4 shows that the return probability is slightly greater than 0.5 just above the threshold of sustained self-sputtering, and it decreases as the discharge is driven further from the threshold by using higher discharge voltage.

The fact that the ion current can exceed the discharge current is not contradicting Kirchhoff's law because we consider two circuits: the discharge circuit and the bias circuit. The discharge circuit provides the ions needed to transport current in the second circuit. To further understand the system, we should consider the energy balance or equivalently, in steady state, the power balance. The majority of copper ions is singly charged (own unpublished data, and [23]), with typically several percent doubly charged, and so it is acceptable to approximately balance the

energy provided by secondary electrons with the energy needed to produce singly charged ions (a generalization to include doubly charged ions is straight-forward but makes the consideration less transparent):

$$I_{SE}\, U_{sheath} \geq \left(\frac{I_{disch}}{1+\gamma_{SE}} + \frac{I_{collect}}{1+\gamma_{SE}} + I_{i,lost} \right) \frac{E_i}{e} \,. \tag{12}$$

The *l.h.s.* of (12) is the input power, with the secondary electron current $I_{SE} = I_{disch}\, \gamma_{SE} / \left(1+\gamma_{SE}\right)$, and U_{sheath} representing the sheath voltage (one can assume that this is a large fraction of the applied voltage, e.g. $U_{sheath} \approx 0.8\, U$). The *r.h.s.* represents the flux of all ions times the effective ionization energy. We can simply use the first ionization energy, $E_i = E_{01} = 7.73$ eV and neglect the small contribution of the ion current not going to the target or ion collector, $I_{i,lost}$, to arrive at

$$\gamma_{SE} \geq \frac{\left(I_{disch} + I_{collect}\right) E_{01}}{e\, I_{disch} U_{sheath}} \,. \tag{13}$$

All of those quantities are known, and a numerical evaluation shows that $\gamma_{SE} \geq 0.033$ for the range of voltages and currents of our experiment. The small value of γ_{SE} justifies, *a posteriori*, some assumptions previously made.

Next, using the approximate electron temperature of 3 eV, and the area of the ion collector, we can estimate the average plasma density at the collector's sheath edge to be about 2×10^{18} m^{-3} when the collector current is about 100 A – also this value is reasonable and consistent with the previous estimates of the ionization rates.

Secondary electrons heat the electrons by momentum exchange collisions, which is very effective due to the Coulomb interaction and the matching of the electron mass. Spitzer [24] determined that the thermalization time for an energetic electron is approximately

$$\tau_{thermal} \approx \frac{2\pi\, \varepsilon_0^2\, v_e^3\, m_e^2}{e^4\, n_e\, \ln\Lambda} \tag{14}$$

where v_e is the initial electron velocity and $\ln\Lambda \approx 10$ is the Coulomb logarithm. Most of the thermalization occurs in the dense plasma near the target, and one can find that the typical time for thermalization is several 10 μs, which is of the same order of magnitude the system needs to go to steady state.

In summary, we have demonstrated, both theoretically and experimentally, that self-sputtering in vacuum can deliver extraordinarily high metal ion current. The usable ion current increased exponentially with increasing discharge voltage, which was shown to be associated with an increase in the ionization rate and a reduction of plasma confinement as the voltage was increased. In the experiments with copper in vacuum, the highest ion current demonstrated was 250 A, far exceeding any comparable attempt.

This work was supported by the Wenner-Gren Foundations, Sweden, and the Assistant Secretary for Energy Efficiency and Renewable Energy, Office of Building Technology, of the U.S. Department of Energy under Contract No. DE-AC02-05CH11231.

[1] A. Anders, *Cathodic Arcs: From Fractal Spots to Energetic Condensation* (Springer, New York, 2008).

[2] V. Kouznetsov *et al.*, Surf. Coat. Technol. **122**, 290 (1999).

[3] K. Macak *et al.*, J. Vac. Sci. Technol. A **18**, 1533 (2000).

[4] U. Helmersson *et al.*, Thin Solid Films **513**, 1 (2006).

[5] J. Bohlmark *et al.*, Thin Solid Films **515**, 1522 (2006).

[6] N. Hosokawa, T. Tsukada, and T. Misumi, J. Vac. Sci. Technol. **14**, 143 (1977).

[7] N. Hosokawa, T. Tsukada, and H. Kitahara, in Proc. 8th Int. Vacuum Congress, Le Vide, Cannes, France, 1980), pp. 11.

[8] W. M. Posadowski, and Z. Radzimski, J. Vac. Sci. Technol. A **11**, 2980 (1993).

[9] S. Kadlec, and J. Musil, Vacuum **47**, 307 (1996).

[10] A. Anders, J. Andersson, and A. Ehiasarian, J. Appl. Phys. **102**, 113303 (2007).

[11] A. Anders, J. Andersson, and A. Ehiasarian, J. Appl. Phys. **103**, 039901 (2008).

[12] J. Andersson, and A. Anders, Appl. Phys. Lett. **92**, 221503 (2008).

[13] D. Bohm, in *The Characteristics of Electrical Discharges in Magnetic Fields*, ed. by A. Guthrie, and R. K. Wakerling (McGraw-Hill, New York, 1949), 77.

[14] P. M. Chung, L. Talbot, and K. J. Touryan, *Electric Probes in Stationary and Flowing Plasmas: Theory and Applications* (Springer, Berlin, 1975).

[15] K.-U. Riemann, J. Phys. D: Appl. Phys. **24**, 493 (1991).

[16] L. M. Biberman, V. S. Vorobev, and I. T. Yakubov, *Kinetics of the Non-Equilibrium and Low-Temperature Plasma (in Russ.)* (Nauka, Moscow, 1982).

[17] Y. P. Raizer, *Gas Discharge Physics* (Springer, Berlin, 1991).

[18] D. J. Christie, J. Vac. Sci. Technol. A **23**, 330 (2005).

[19] J. Vlček *et al.*, J. Vac. Sci. Technol. A **25**, 42 (2007).

[20] J. A. Hopwood, *Ionized Physical Vapor Deposition* (Academic Press, San Diego, CA, 2000).

[21] H. Eder *et al.*, J. Appl. Phys. **87**, 8198 (2000).

[22] A. Anders, Appl. Phys. Lett. **92**, 201501 (2008).

[23] J. Vlček *et al.*, Eur. Phys. Lett. **77**, 45002 (2007).

[24] L. Spitzer Jr., *Physics of Fully Ionized Gases* (Dover, New York, 1990).

Fig. 1 (color online). Electron impact ionization and three-particle recombination rates for copper plasma as a function of electron temperature.

Fig. 2 (color online). Current to the ion collector as a function of time for different bias voltages ("gasless" sputtering of copper at 800 V, steady-state discharge current of 68 A, in 10^{-4} Pa background pressure).

Fig. 3 (color online). Ion collector current from a copper magnetron discharge in vacuum as function of time, with the discharge voltage as a parameter, at a constant collector bias of -30 V.

Fig. 4 (color online). Discharge current and ion collector current as a function of the discharge voltage. Both currents show exponential growth with the correlation coefficients $R^2 = 0.996$ for the discharge current and $R^2 = 0.998$ for the ion current. The arrow at 666 V indicates when the collector current equals the discharge current. The return probability, β, was calculated from the ratio of discharge current and collector current as explained in the text.

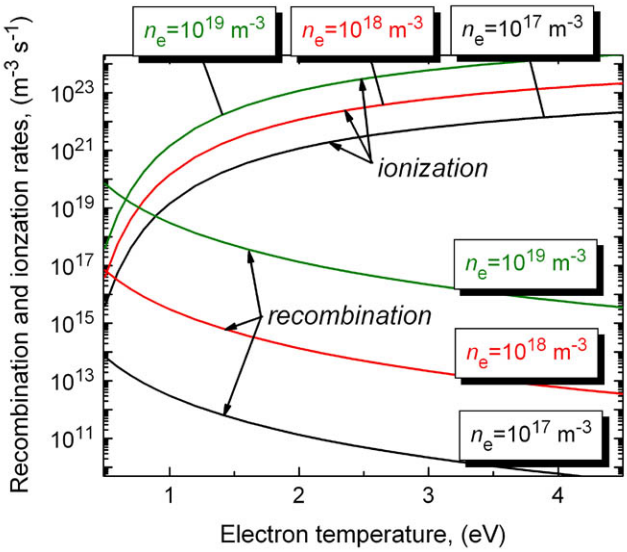
n_e=10^{19} m^{-3}
n_e=10^{18} m^{-3}
n_e=10^{17} m^{-3}
ionization
recombination
n_e=10^{19} m^{-3}
n_e=10^{18} m^{-3}
n_e=10^{17} m^{-3}
Recombination and ionzation rates, (m^{-3} s^{-1})
10^{23}
10^{21}
10^{19}
10^{17}
10^{15}
10^{13}
10^{11}
1
2
3
4
Electron temperature, (eV)

Fig. 1

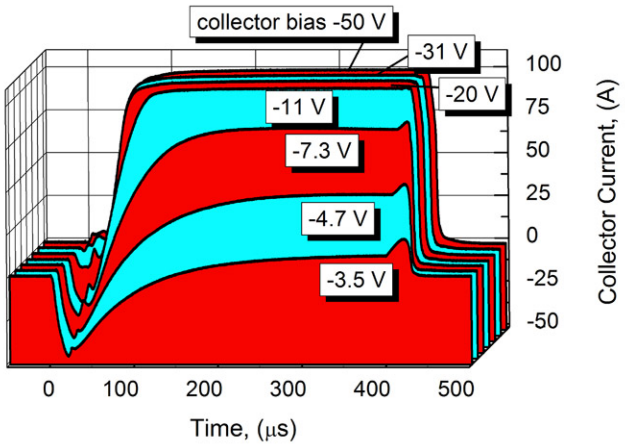
collector bias -50 V
-31 V
-20 V
-11 V
-7.3 V
-4.7 V
-3.5 V
100
75
50
25
0
-25
-50
Collector Current, (A)
0
100
200
300
400
500
Time, (μs)

Fig. 2

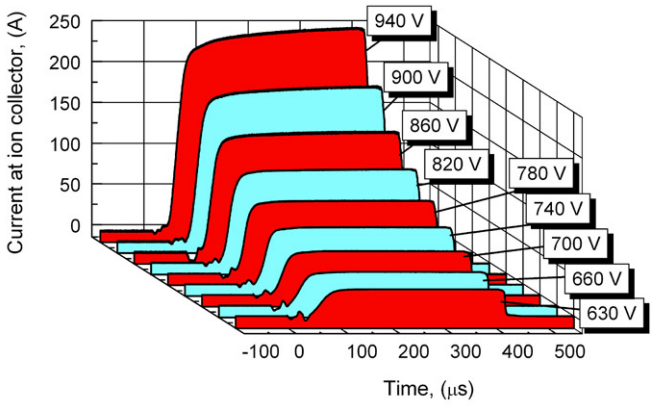
Current at ion collector, (A)
250
200
150
100
50
0
940 V
900 V
860 V
820 V
780 V
740 V
700 V
660 V
630 V
-100
0
100
200
300
400
500
Time, (μs)

Fig. 3

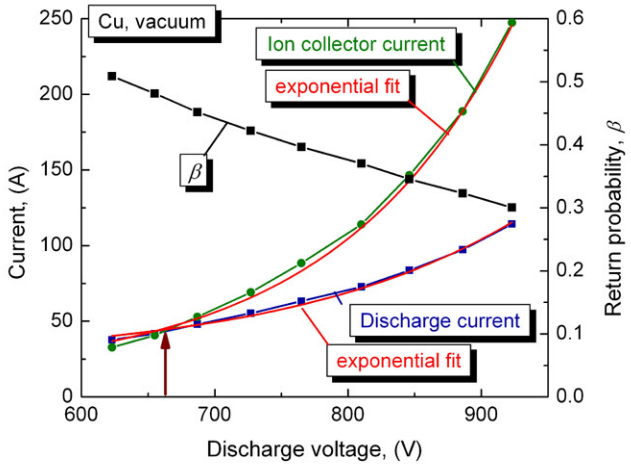
Cu, vacuum
Ion collector current
exponential fit
β
Discharge current
exponential fit
Current, (A)
Return probability, β
Discharge voltage, (V)
250
200
150
100
50
0
600
700
800
900
0.6
0.5
0.4
0.3
0.2
0.1
0.0

Fig. 4